DOI: 10.1002/ejic.201200626

The Mechanical Performance of a Biomimetic Nanointerface Made of Multilayered Polyelectrolytes

Sacha Cavelier,[a] Christopher J. Barrett,[b] and Francois Barthelat*[a]

Keywords: Materials science / Nanostructures / Layered compounds / Organic–inorganic hybrid composites / Thin films / Mechanical properties / Polyanions / Polycations

Integrating organic and inorganic components into hybrid materials is a promising pathway towards unique and useful combinations of stiffness, strength, and toughness. Nature provides superb examples of such materials: bone, teeth, and mollusk shells are made of stiff inorganic mineral inclusions bonded by more compliant proteins and polysaccharides that play a critical role by providing large deformations and energy absorption. Nanometer-thick polyelectrolyte multilayers (PEMs) provide an elegant approach to mimicking natural organic materials, but experimental data on their mechanical properties is scarce. In this work we have for the first time measured the shear performance and fracture toughness of PEM nanointerfaces that join two silicon substrates. Most of the properties of PEMs fall between those of a typical office tape and an engineering epoxy. However, the energy for failure in shear in PEMs exceeds the other two adhesives by far, because of breakage and reformation of electrostatic bonds. Interestingly, the properties of PEMs can be tuned by, for example, depositing a preliminary (3-aminopropyl)triethoxysilane layer or by adjusting the degree of hydration. They can also partially heal, and we demonstrate how only a fraction of the initial toughness is lost upon reassembly after fracture. This set of mechanical properties will greatly facilitate the design and optimization of future hybrid materials inspired from nature.

Introduction

Hybrid materials provide a powerful approach to expanding the range of properties of materials,[1] and this type of material therefore continues to excite the curiosity of engineers, materials scientists, physicists, and chemists.[2] The efficacy of hybrid materials is fully harnessed when the two or more components of which they are made have strongly contrasting properties, as is the case for organic (soft, ductile, low strength) and inorganic (stiff, strong, but brittle) hybrids. Well-designed inorganic–organic hybrid materials can then achieve unusual combinations of stiffness, strength, and toughness by using the stiffness of the inorganic phase (mineral or ceramic) with the large deformation and energy dissipation of the organic phase (polymers). Impressive examples of such materials are found in nature: bone, teeth, and seashells consist of soft organic matrices (proteins and polysaccharides) reinforced by stiff inorganic mineral inclusions. The biological materials cover a remarkable range of stiffness, strength, and toughness,[3] despite the fact that they use only a few "universal" nanoscale building blocks such as collagen type I or cellulose.[4] Proteins are soft in the hydrated state, so a typical strategy consists of incorporating minerals to increase stiffness and strength.[5] In extreme cases such as tooth enamel or sea urchin spines, mineral content exceeds 99%, but there is always a small portion of organic materials to guide cracks, control failure, and dissipate energy.[6,7] These materials boast outstanding mechanical performance, and they have therefore become a significant source of inspiration for the design and fabrication of new high-performance engineering materials. Mimicking the structure and properties of these materials presents significant challenges. In particular, tight control of the microstructure is difficult, and we have yet to duplicate the remarkable properties of natural organic materials (large deformation, energy dissipation through molecular sacrificial bonds, nanoscale structures). Amongst natural hybrid materials, nacre, the iridescent layer found inside mollusk shells, has been one of the most studied. Nacre is made of 95 vol.-% microscopic tablets of calcium carbonate bonded by nanometer-thick interfaces of softer proteins and polysaccharides (Figure 1, a). Because of its high mineral content, nacre is stiff and strong, and also, despite the brittleness of mineral, nacre is extremely tough, 3000 times tougher than the mineral itself.[8] No such "toughness amplification" has been achieved to date in engineering materials. This performance is the result of well-controlled mechanisms at the microscale, which consist of the sliding of the tablets on one another under tensile loading (Figure 1, b).

[a] Department of Mechanical Engineering, McGill University, 817 Sherbrooke Street West, H3A 2K6 Montreal, Quebec, Canada
E-mail: francois.barthelat@mcgill.ca
Homepage: http://barthelat-lab.mcgill.ca/
[b] Chemistry Department, McGill University, 817 Sherbrooke Street West, H3A 2K6 Montreal, Quebec, Canada

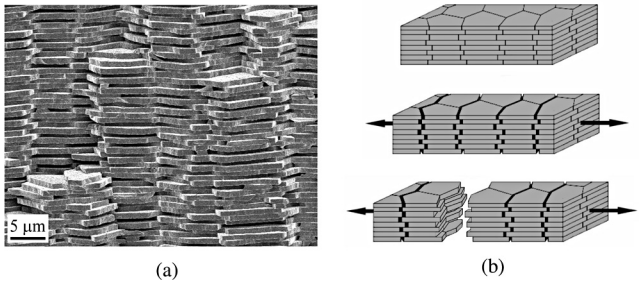

Figure 1. (a) The brick-and-mortar microstructure of natural nacre and (b) the deformation mechanism in natural nacre (adapted from the literature[9]).

This process dissipates energy through viscoplasticity at the interface, which leads to tremendous amplification of toughness at the macroscopic scale.[8] In the process, the tablets themselves remain elastic and their function is to carry tensile stress and stiffen the structure, as well as to confine the organic interfaces. In light of this example, it becomes evident that the properties of the material are highly dependent on the properties of the interfaces themselves.[10,11] In nacre, the interfaces can withstand tremendous amounts of shear deformation and dissipate energy in the process. Some of the proteins present in the interfaces have "hidden lengths" along their molecular chain that can unfold upon the breakage of sacrificial bonds.[12] This process generates extra lengths for the proteins to unfold, which results in large extensibility and the dissipation of mechanical energy. The duplication of these structures and mechanisms has proven extremely challenging. Amongst the various polymers that have been used as interfaces for "nacrelike" materials, polyelectrolyte multilayers (PEMs) might be the most promising because they can duplicate some of the attributes of the interface in natural nacre.[13] These electrically charged polymers can be self-assembled into nanometer-thick multilayers (Figure 2, a) that are extremely stable and durable, their thickness can be adjusted in the nanometer range,[13] and their mechanical properties can be easily tuned by, for example, modifying the pH during deposition. pH has an important effect on the structure of PEMs; it affects thickness, film morphology, and surface roughness.[14] These variations in turn have profound effects on mechanical properties including modulus or coefficient of friction of the deposited film. The electrostatic interactions that provide the cohesion of the layers can form and reform reversibly when the interface is deformed, thereby proving cohesion over a large range of deformation (as demonstrated by Kotov et al.,[13] for example). In addition, polyelectrolytes can be used to drive layer-by-layer self-assembly,[2,15] which can be used to generate nacrelike microstructures (Figure 2, b). An efficient fabrication technique does not, however, in itself guarantee the success of a material, and it is now well known that the microstructure of nacrelike material must be fine-tuned to achieve a nacrelike-type deformation (Figure 1, b). In particular, it is important to carefully tailor the microstructure and properties of the interfaces to ensure that the inclusions will slide on one another instead of fracturing.[8,16–18] In this context, accurate knowledge of the mechanical properties of the interfaces is critical. Numerical simulations performed by Cranford et al. have already shown that pH has an important impact on the PEMs, and the range 7 to 8 is optimum to obtain a consistent PEM film.[19] The absorbance, roughness, stability, and friction of PEMs were studied by Dai et al.[20] The elastic behavior of PEMs was studied by using atomic force microscopy,[21] nanoindentation,[22] or mechanical experiments on microcapsules made of PEMs.[23,23b,24] The Young moduli found in these experiments ranged from 60 to 200 MPa. Some of these studies also demonstrated the impact of the molecular weight of the PEMs and also how heat treatment can change the nature of the linkage from ionic to covalent bonding. Other techniques included the use of a dissipative quartz crystal microbalance to measure the shear modulus, as performed recently by Guzman et al. on ultrathin PEMs of sodium salt.[25] Despite these recent advances in our knowledge of the mechanical response of PEMs, basic data on shear and adhesive strength are still missing. Material design and optimization with PEMs is therefore difficult, because the elas-

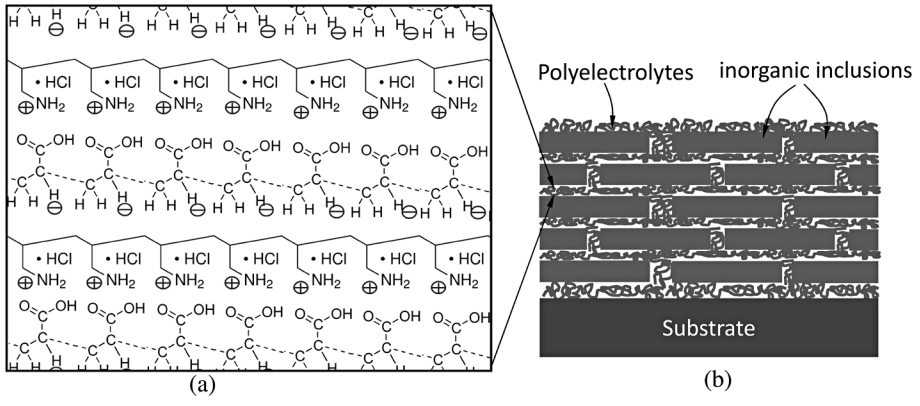

Figure 2. (a) Molecular structure of polyelectrolyte multilayers (PEMs) and (b) schematic illustration of an organic–inorganic hybrid material mimicking natural nacre using PEMs (adapted from the literature[13]).

tic parameters are insufficient to properly design and optimize a nacrelike hybrid material. In this work we have addressed this lack by measuring, for the first time, the shearing and fracture performance of PEMs.

Preparation of Multilayered Polyelectrolyte Interfaces

Silicon is an inorganic material that is often combined with polyelectrolytes,[26] and for this reason we have chosen single-crystal silicon wafers as substrates for the polyelectrolyte multilayers (PEMs). Thin strips of silicon with dimensions of 17 by 3.5 mm were cut from a 0.5 mm-thick silicon wafer by diamond scribe and cleaving. The substrates were then cleaned by immersion in a Piranha bath (H_2SO_4, product no. 339741, Sigma–Aldrich, Buchs, Switzerland) for 20 min and at 60 °C.[7] Oxygen peroxide (H_2O_2, product no. 31642, Sigma Aldrich, Buchs, Switzerland) was added after 20 min to agitate the solution and to promote the formation of an oxide layer on the silicon strips. After 30 min of immersion, the strips were removed and washed with Milli-Q (deionized and highly purified) water. Before the deposition of PEMs, some of the samples were treated with (3-aminopropyl)triethoxysilane (APTES, product no. 281778, Sigma Aldrich, Buchs, Switzerland). APTES loses its three ethyl groups to form a strong covalent attachment on the silicon oxide.[27] Another ethyl group is lost and replaced by a positively charged NH_3^+ group suitable to accept a first layer of negatively charged polyelectrolyte. The procedure for APTES-treated samples was to completely dry the silicon strips and submerge the tablets in a APTES diluted solution (2% APTES anhydrous solution for 98% ethanol) for 90 min,[27] followed by sonication in pure toluene (twice for 10 min) to remove loosely physisorbed APTES. The strips were then dried again and placed in an oven at 100 °C for two hours to cure the APTES. After curing, the strips were sonicated in milliQ water (three times for 10 min each).

Prior to the actual PEM deposition and for all samples (APTES and non-APTES), one end of the strips was wrapped in a mask of Teflon tape over a length of 5 mm. The masks were used to hold the strips during the PEM deposition process, and to restrict the deposition to a predetermined section of the strip (Figure 3). Sequential baths of a negatively charged polyelectrolyte in solution [0.01 mol L^{-1} polyacrylic acid (PAA), Sigma Aldrich, Buchs, Switzerland] and a positively charged polyelectrolyte [0.01 mol L^{-1} polyallylamine hydrochloride (PAH), Sigma Aldrich, Buchs, Switzerland] alternated with three milliQ rinsing baths were prepared on a cycling robot (Shandon Varistain auto slide stainer, Princeton, NJ). Since the surface of the silicon strip tends to be negatively charged, the first bath was in positively charged PAA for 10 min, followed by three rinsing baths of milliQ at 2 min each, followed by a 10 min bath of negatively charged PAH and three 2 min rinsing baths (Figure 3, a). This formed first a polyelectrolyte bilayer on the surface of the silicon strip (Figure 3, b). The process was repeated to achieve the minimum of 40 bilayers required to obtain a stable, continuous coating on each strip.[28,29] The pH of the deposition solutions has a profound effect on the structural properties of

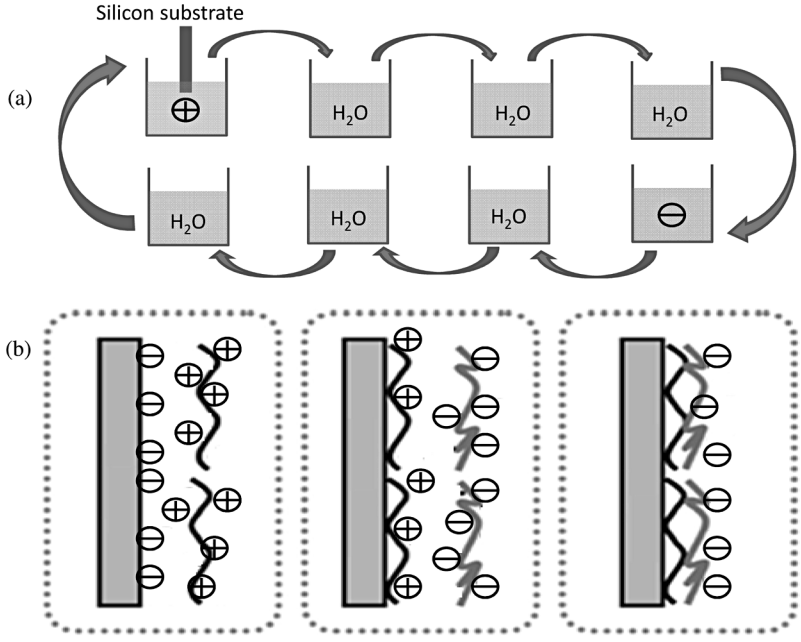

Figure 3. (a) Summary of the chemical protocol to coat a silicon tablet with several positive and negative polyelectrolyte layers. (b) Schematic illustration of the deposition of the positive and negative polyelectrolyte molecules on the silicon tablet.

PEMs. In this work, the pH was chosen to generate the largest electrostatic attractions (i.e., the maximum net ionization) to obtain the highest mechanical strength. A neutral pH of 7 was therefore chosen for both positive [polyallylamine hydrochloride (PAH)] and negative [polyacrylic acid (PAA)] polyelectrolyte solutions.[19] The thickness of the coating was measured on a few strips by using ellipsometry,[14] and we found that it ranged from 150 to 300 nm. The first ten deposited bilayers are highly disorganized, and only the bilayers deposited thereafter show a clear layered structure.[14] The layer structure itself is not perfectly flat but wavy, and its waviness is partially controlled by the more random structures of the first ten layers. The variability in the thickness might therefore result from local variations in the structure of the PEMs. The multilayer deposition process ended with a negatively charged polyelectrolyte layer for all strips, after which half of the strips were coated with a final positively charged layer. Pairs of negatively/positively charged strips were then manually assembled individually in milliQ water to produce the testing samples, which followed either the shear lap or double cantilever beam configurations described in the next sections. The two silicon substrates were carefully aligned against a ruler to ensure that they were parallel to each other. Adhesion was promoted by applying a fixed weight for about 12 hours on the two strips in milliQ water, which corresponded to a normal pressure of about 3 kPa on the interface. The interface between the silicon substrates were therefore composed of 80 bilayers of polyelectrolytes for an average thickness of 440 nm. After assembly the samples were stored in milliQ water until testing.

Shear Deformation and Failure

Shearing is a common deformation and failure mode for biological and engineering adhesive. To characterize the performance of adhesives in shear, the shear lap test (Figure 4) is widely used.[30] Here we have adapted this technique to test small-scale samples. After the silicon strips were assembled, additional tabs were glued at the ends of the samples to minimize bending moments. To deform and fracture the interface in shear, a tensile force was applied at the ends of the sample by using a horizontal miniature loading machine[31] with a 25 N load cell. A large quantity of milliQ water was applied to the surface of the sample to maintain the interface hydration during the test.

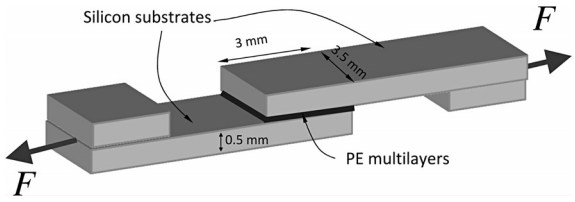

Figure 4. The single-lap shear test configuration with relevant dimensions.

To prevent spurious transverse force, bending moments, and torque, flat mats of flexible carbon fibers were used to transmit exclusively tensile forces to the specimen. An optical setup was also used to accurately measure the displacements associated with the shearing of the interfaces. To this end, a tab cut from the silicon wafer was first glued onto the lower strip of the sample to serve as reference for displacement measurements (Figure 5, a). The testing machine with the mounted sample was then placed under an upright, reflected light microscope[31] to measure the relative displacement between the reference block and the upper strip of the sample (Figure 5, a). Digital images were acquired during the test and processed by using digital image correlation (DIC), an automated process that tracks the displacements of each pixel from one image to another. This method relies on the presence of dark and light features

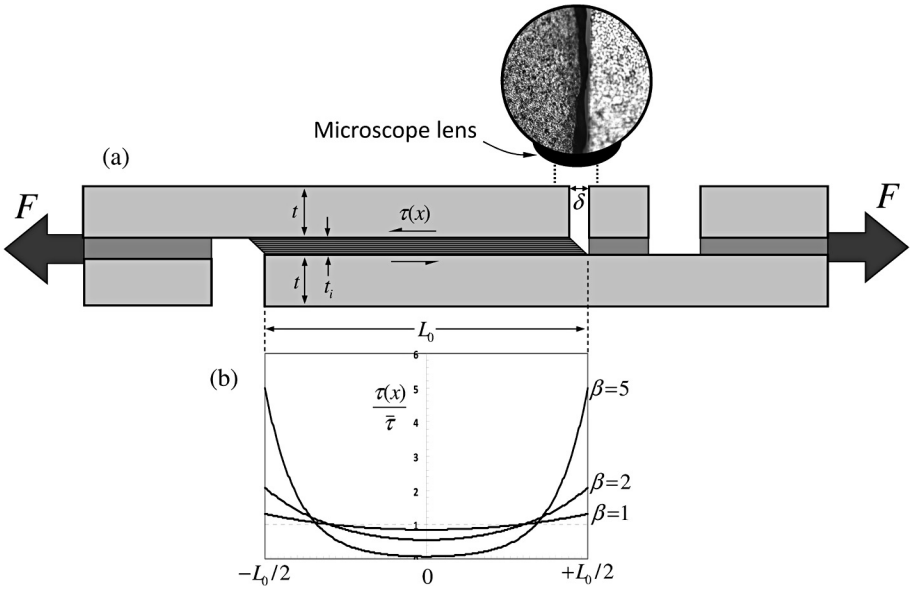

Figure 5. (a) Shear lap testing setup showing optical measurement of the sliding distance δ. (b) Profile of shear stress as function of the nondimensional parameter β.

with sufficient contrast on the surface of the specimen, and in this case the roughness of the rear surface of the silicon wafer provided an adequate black and white speckle for DIC analyses (Figure 5, a). The resulting displacements in pixels were then converted to micrometers.

Figure 6 shows a set of force/displacement curves for the shear lap tests (displacement measurements were only possible on three samples). The curves are essentially linear, and the failure is brittle. No sign of nonlinearities or stable crack propagation was observed. Although the curves show consistent initial slopes, they display large variations in strength. More samples were tested to measure strength only.

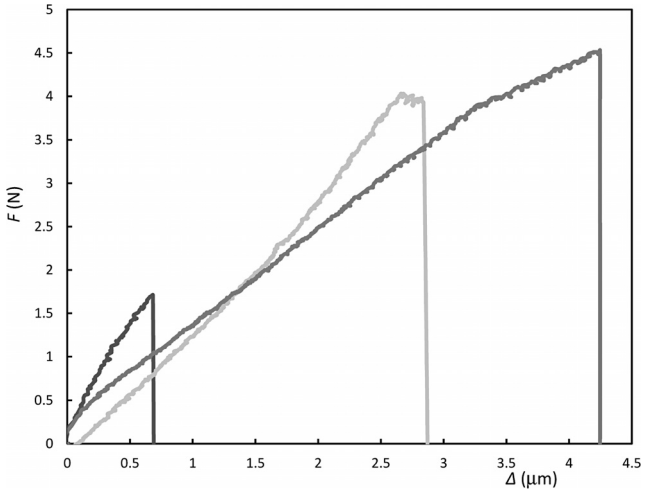

Figure 6. Typical force (F)/displacement (Δ) curves obtained from the shear lap test.

Although the experimental setup of the lap shear test is relatively easy to implement, the analysis is more complicated because the shear stress transmitted by the interface is not necessarily uniform. An early analysis from Volkersen[32] (also summarized in the literature[33]) examined the transfer of stress across the interface, assuming that the prominent deformation modes are tensile for the substrates and shear for the interface. This analysis leads to distribution of shear stress along the interface [Equation (1)]

$$\frac{\tau(x)}{\bar{\tau}} = \beta \frac{\cosh\left(2\beta\frac{x}{L_0}\right)}{\sinh\beta} \quad \text{with} \quad \beta = \frac{L_0}{t}\sqrt{\frac{1}{2}\frac{G_i}{E}\frac{t}{t_i}} \tag{1}$$

in which x is the position along the interface, L_0 and t_i are the length of the interface, t is the thickness of each of the substrates, E is the Young's modulus of the substrates, and G_i is the shear modulus of the interface. This result is standard, but here we have defined the parameter β as a nondimensional number that makes it easier to interpret the model. The profile of shear stress along the interface (normalized by the average shear stress $\bar{\tau} = F/wL_0$) for different values β is shown in Figure 5 (b). In general, the shear stress is not uniform and the stresses are concentrated at the ends of the interface. This effect is more pronounced for higher values of β, in other words, with relatively stiff interfaces compared to the substrates (high $\frac{G_i t}{E t_i}$ ratio) and/or longer normalized interface length $\frac{L_0}{t}$. In the extreme cases, all of the shear stress is transferred near the ends of the interfaces, and the shear stresses anywhere else are zero. On the other hand, the shear stress is more uniform for small values of β, which correspond to relatively soft interfaces and/or short interface lengths. For $\beta = 0.4$ or lower, the shear stress deviates from its average value by 5% at most. The value of β is therefore the critical factor that determines how the shear is transferred through the interface, and how shear modulus and shear strength can be extracted from the experimental curves. Although β is not accessible a priori, it can be computed from the slope of the force/deflection curve. The maximum shear stress is [Equation (2)]

$$\tau_{\max} = \tau\left(x = \frac{L_0}{2}\right) = \beta\frac{F}{wL_0}\frac{1}{\tanh\beta} \tag{2}$$

and it occurs at the end of the interface, where the displacement δ is measured experimentally (Figure 5, a). Using Hooke's law for the elastic interface leads to an expression for the slope of the force/deflection curve [Equation (3)].

$$\frac{dF}{d\delta} = \frac{wL_0G_i}{t_i\beta}\tanh\beta \tag{3}$$

For the present experiments, $w = 3.5$ mm, $t = 500$ μm, $L_0 = 3$ mm, $t_i = 440$ nm, and $E \approx 130$ GPa for silicon lead to shear moduli in the range of 100–400 kPa for the interfaces. Equation (1) predicts $\beta \approx 0.005$–0.01, and these low values therefore indicate that the shear stress is uniform along the interface. The equations become, for $\beta << 1$[$\sinh\beta \approx \beta$, $\tanh\beta \approx \beta$, $\cosh(2\beta\frac{x}{L_0}) \approx 1$] [Equation (4)].

$$\begin{cases} \tau(x) = \bar{\tau} \\ \tau_{\max} = \dfrac{F}{wL_0} \\ G_i = \dfrac{t_i}{wL_0}\dfrac{dF}{d\delta} \end{cases} \tag{4}$$

The shear strength and the shear modulus of the interface can then be easily computed by using Equation (4), and the shear strain at failure can also be evaluated using Equation (5).

$$\gamma_f = \frac{\delta_f}{t_i} \tag{5}$$

The results are shown in Figure 7. For comparison we also show the shear modulus and shear lap strength of a weak adhesive (standard double-sided office tape) and a strong engineering adhesive (epoxy on glass). We chose office tape because virtually everyone has a sense of how diffi-

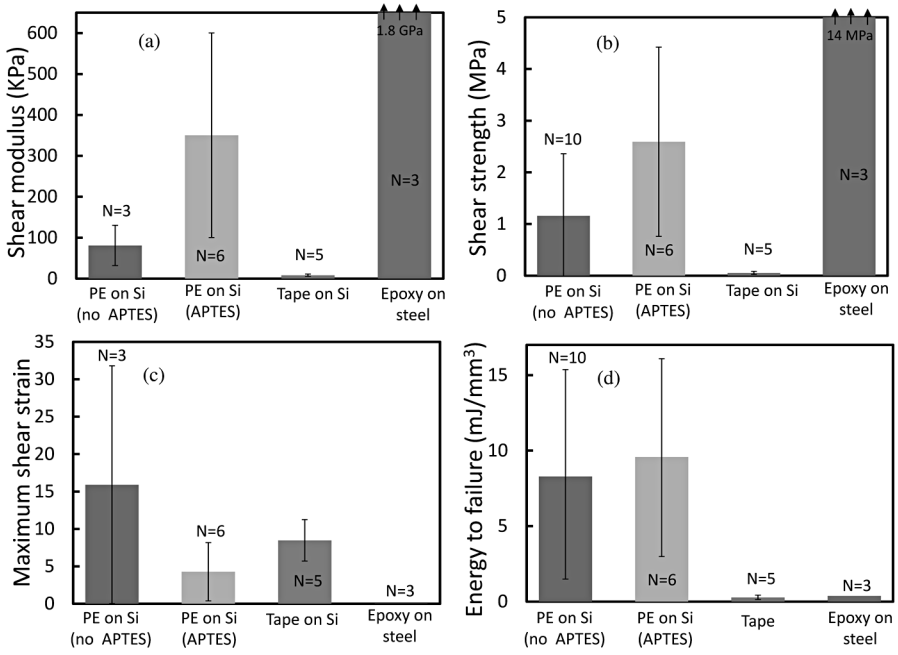

Figure 7. Summary of the results for the shear lap on PE layers on silicon, with and without APTES for (a) shear modulus (p = 0.024), (b) shear strength (p = 0.016), (c) shear strain at failure, and (d) energy to failure. A comparison with a weak adhesive (double-sided office tape) and a strong adhesive (epoxy) is also shown.

cult it is to peel tape off a glass surface, and epoxy because it is one of the most common engineering glues used nowadays. The number of specimens N tested for each configuration is also specified. Values of p were used to characterize whether the differences between different configurations are statistically significant.

A first observation is that the standard deviation of this data is significant, despite our efforts to fabricate and test the samples uniformly. This could be attributed to insufficient control of the multilayered structure at the nanoscale, and to statistics related to the electrostatic interactions. Nevertheless, the results enabled us to draw important conclusions about the behavior of the PE multilayers in shear. First, PE multilayers are about 20 times stiffer and 10 times stronger than office tape on silicon, but about 6 times softer and 3000 times weaker than epoxy on steel. Indeed, PEMs as adhesives are unknown, whereas epoxy is a widely used strong glue and tape is a weak glue that everybody uses and has an idea of the mechanical properties. Therefore displaying the properties of tape and epoxy will help to better understand in which range the performance of the PEMs fall. The APTES treatment prior to PE deposition had a significant impact on mechanical properties: PEMs with APTES treatment were three times stiffer and two times stronger than PE layers deposited without APTES treatment. Figure 7 (c) shows the shear strain at failure, which was 3 times larger for non-APTES samples. The shear strains are extremely high (1500%) and along the order of the strains observed in office tape, in which viscous flow of the acrylic adhesive layer dominates in shear. It is probably the ability of the PE layers to slide on one another, combined with the capability of the electrostatic interaction to break and reform, which give PEMs this tremendous shear deformation capability. Whereas APTES-treated samples are stiffer, their shear strain at failure is smaller than non-treated samples, so that the energy to failure (area under the shear stress/strain curve) is similar for both treated and untreated samples (Figure 7, d). The energy to failure in shear is high: 20 times greater than the energy of tape or epoxy (Figure 7, d). It is mainly due to the low value of the shear strength for the tape and it is a consequence of the low shear strains of epoxy. The difference in properties between APTES and non-APTES samples was explained by an examination of the fracture surfaces. Figure 8 (a) shows an optical micrograph of the PE layers before assembly, and after the shear lap testing for those with APTES (Figure 5, a) and without APTES (Figure 5, b). For those without APTES, the rough surfaces suggest delamination and a mixed cohesive/adhesive mode of failure. Formation of ligaments during the shear process might increase the strain at failure and add to overall toughness. On the other hand, APTES-treated samples displayed a smooth fracture surface. The adhesion of the PEMs on silicon was stronger, so that cohesive failure (between PEMs layers) prevailed. Whereas the strength was to be higher than the untreated samples, limited toughening mechanisms and a more brittle type of failure led to smaller strain at failure. In these optical images, the iridescent appearance of these surfaces was generated by interference between light rays reflected on the surface with light reflected from interfaces beneath the surface. Similar effects are observed with natural nacre and PE-based nanocomposites.[13]

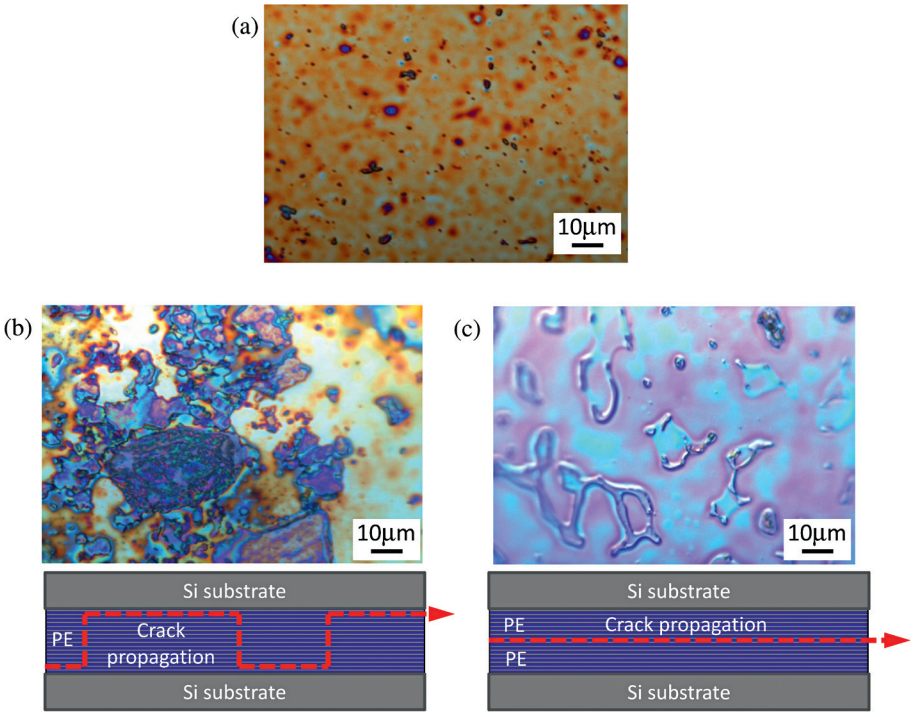

Figure 8. Optical micrograph of (a) pristine PEMs before assembly of the silicon strips; fracture surfaces of (b) silicon tablet coated with PEMs (untreated); and (c) silicon tablet coated with PEMs treated with APTES. The schemes illustrate the propagation modes for each case.

Mode I Fracture Toughness

Another important characteristic of engineering adhesives is their "peeling strength", for which a more appropriate term might be mode I fracture toughness (opening mode). A typical experimental setup to measure interfacial toughness is the double cantilever beam, or DCB.[34] Here again we have scaled down the dimensions of a typical DCB sample to test the interface of the PE layers between two silicon strips, and we used the setup shown in Figure 9. After assembly, the PEMs only covered a section of the surface of the silicon strips, so that the free section of the strips formed two cantilevered beams (hence the name of the test). An opening force was applied at the ends of the strips through pins and two tubes (Figure 9), thus generating an opening stress on the interface. All tests were performed at a displacement rate of 5 µm s^{-1}, and an abundant quantity of milliQ water was applied to the samples to maintain a hydrated interface.

Figure 10 shows typical resulting force/displacement curves for this test. All non-APTES-treated samples displayed the characteristics of a "pop-in" type of fracture in which the crack suddenly propagates but is arrested shortly thereafter. Each drop on the curves of Figure 10 corresponds to a crack advance, and each sample displayed 3 to 4 of these drops, including the final drop, which led to complete failure of the sample. In contrast, APTES-treated samples displayed a brittle type of failure (Figure 10). In this work we used the work of fracture (wof) as a measure

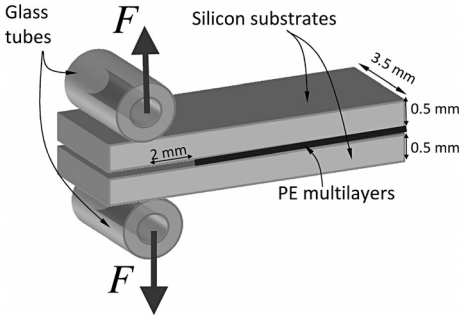

Figure 9. The double cantilever beam test configuration with relevant dimensions.

of the toughness of the interface by dividing the area under the force/deflection curve by the surface area of the PE interface.

Figure 11 (a) displays a summary of the results. As previously, the series have been analyzed statistically on account of the p value. A first observation is that the standard deviation of this data is again significant, but the experiments nevertheless provide a good estimate for toughness. The range of toughness for PE is 1–10 J m^{-2}. For comparison, this is about three times tougher than double-sided tape on silicon, but three times weaker than epoxy on steel. As in the shear tests, we found that the fracture toughness of APTES-treated samples is actually lower than untreated samples (confirmed by a low p value), whereas the fracture surfaces of treated and untreated samples displayed exactly

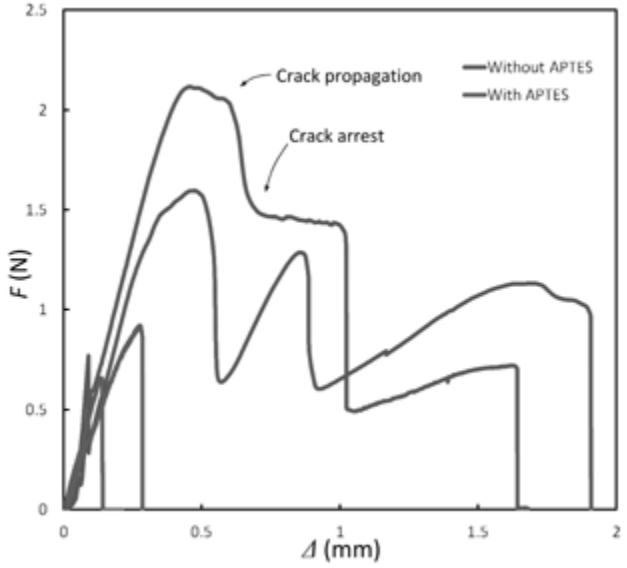

Figure 10. Typical force (*F*)/displacement (Δ) curve obtained from the DCB test.

the same characteristics as in shear (Figure 8, b). This confirms that the mixed fracture mode of untreated samples actually dissipates more energy than APTES-treated samples, which are stronger but more brittle.

The DCB experiments and data analysis are more straightforward than the shear lap test, and therefore we used the DCB experiment to explore the effects of various fabrication and testing conditions. For example Figure 11 (b) shows the effect of applying pressure to the PE interface (without APTES treatment) during assembly, which we found detrimental to toughness for the range of pressures explored. Higher pressure possibly disrupts the layered structure of the PE interfaces and leads to a decreased performance, but we cannot conclude that this difference is significant since the p value ($0.27 > 0.05$) is high. The effect of hydration on the properties of the PE layers was also explored. For this experiment, a group of assembled DCB samples was left to dry overnight and under room-temperature conditions and was tested the next day. Figure 11 (c) shows the effect of hydration on toughness. Dry PEMs are clearly much more brittle than under hydrated conditions (confirmed by a low p value), which could be explained by the water acting as solvent for the PEM molecules, thereby allowing for entropic elasticity and greater flexibility. Another possible explanation is the formation of additional hydrogen bonds between layers under dry conditions, which would reduce ductility and energy dissipation. Finally, Coulomb's law for electrostatic interaction predicts that electric interactions are about 80 times weaker in water than air, because of the difference in permittivity between these two media. Weaker electric interactions lead to lower strength

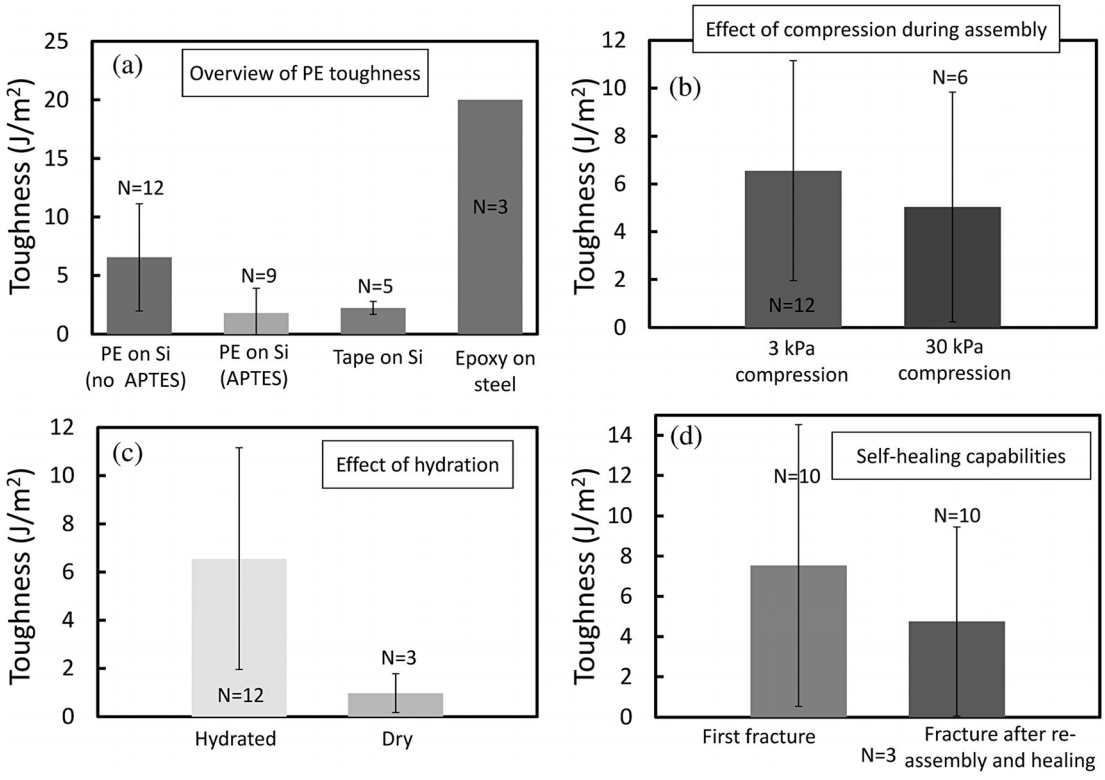

Figure 11. Summary of results for the DCB fracture tests: (a) overview (p value between the two series with and without APTES: $p = 0.003$) and a comparison with a weak adhesive (double-sided office tape) and a strong adhesive (epoxy) is also shown; (b) effect of compression during assembly (3 KPa and 30 KPa, $p = 0.27$); (c) effect of hydration ($p = 0.0008$); and (d) self-healing capabilities ($p = 0.16$).

but also to higher deformability and toughness. Finally, we assessed the healing capabilities of the PE multilayers by reassembly fracture samples after the initial test to test them again using the DCB configuration. The average fracture toughness calculated in the first series (standard samples) is 7.54 $J m^{-2}$ and the average in the second series (repaired samples) is 4.75 $J m^{-2}$. Repaired samples might have reduced toughness but the difference is not statically significant. Although fracturing the PEMs for the first time damaged their structure and led to slightly lower performance after reassembly, these tests clearly demonstrated the partial healing capabilities of the PEMs.

Conclusion

In this work we have characterized for the first time the shear and fracture behavior of polyelectrolyte multilayers (PEMs) that join two silicon substrates. Overall the properties we found were halfway between a weak adhesive (office tape) and strong engineering glues (epoxy), except the energy to failure in shear, which was far greater in PEMs than in the other two adhesives. This is the result of strength on the order of megapascals combined with tremendous shear strains (up to 1500%). These large deformations might be generated by the sliding of individual PE layers over one another and the breakage and reformation of electrostatic interactions by progressive damage accumulation, by nonlinear deformations of wrinkled PE layers, or by entropic elasticity (with water acting as solvent for individual PE molecules). More investigations are needed to assess which of the above deformation mechanisms prevails. Large deformability alone is a property that makes PEMs an attractive material as a mimic of the energy-dissipative proteins found in nacre or bone. Although the shear strength of PEMs is lower than biological interfaces such as those in nacre (25 MPa[9]), the strain at failure is much greater so that the interfacial toughness is the same for PEMs and nacre.[35] The mode I fracture toughness is not as impressive as the energy dissipation in shear, because this fracture mode does not benefit from the breakage and reformation of electrostatic interactions.

The properties of the PEM interfaces can also be easily tuned. For example, the adhesion of the PE layers on silicon can be enhanced by a precursor deposition of APTES, which we found to increase the modulus and strength but decreased toughness. Weaker PE–substrate adhesion promotes cohesive/adhesive mixed mode of failure and possibly generates toughening mechanisms such as crack bridging and energy dissipation. The properties of the PEMs can also be tuned by adjusting the amount of compression during assembly, and by changing the level of hydration. Fracture tests on reassembled PEM interfaces finally demonstrated the partial self-healing capabilities of PEMs. These results are critical for the design and optimization of next-generation biomimetic materials.[8,36] Although the PEM interfaces explored here are probably too thick for applications in nanocomposites,[13] they are relevant to the design and fabrication of larger-scale bioinspired microcomposites made of micrometer-sized ceramic platelets. This size of inclusions is closer to natural nacre, and similar to artificial nacres developed by Bonderer et al.[18] or Deville et al.[37] There are benefits to using thicker interfaces: (1) the first few deposited layers are quite disorganized and a nice multilayered structure can also be achieved after depositing about 10 layers,[14] and (2) the toughness of adhesives in general is known to decrease for smaller thickness, because the volumes that undergo dissipative mechanisms are limited by the spatial confinement of the adherents. These new results for PEMs might also be useful for any other application that relies on the adhesion, strength, or deformation of polyelectrolyte multilayers.

Acknowledgments

The authors would like to acknowledge the help of Zahid Mahimwalla and Miloslav Sailer from McGill Chemistry for the polyelectrolyte deposition training and the coating-thickness measurements by ellipsometry. This research was funded by the Fonds de Recherche du Québec – Nature et Technologies. S. C. was also partially supported by the McGill University, Montreal within the Summer Undergraduate Research in Engineering (SURE) program.

[1] M. Ashby, *J. Am. Ceram. Soc.* **2011**, *94*, S3–S14.
[2] C. Sanchez, H. Arribart, M. M. G. Guille, *Nature Mater.* **2005**, *4*, 277–288.
[3] U. G. K. Wegst, M. F. Ashby, *Philosophical Magazine* **2004**, *84*, 2167–2181.
[4] M. J. Buehler, *Nano Today* **2010**, *5*, 379–383.
[5] J. D. Currey, *J. Exp. Biol.* **1999**, *202*, 3285–3294.
[6] J. Seto, Y. R. Ma, S. A. Davis, F. Meldrum, A. Gourrier, Y. Y. Kim, U. Schilde, M. Sztucki, M. Burghammer, S. Maltsev, C. Jager, H. Colfen, *Proc. Natl. Acad. Sci. USA* **2012**, *109*, 7126–7126.
[7] D. Bajaj, D. D. Arola, *Biomaterials* **2009**, *30*, 4037–4046.
[8] F. Barthelat, R. Rabiei, *J. Mech. Phys. Solids* **2011**, *59*, 829–840.
[9] F. Barthelat, H. Tang, P. D. Zavattieri, C. M. Li, H. D. Espinosa, *J. Mech. Phys. Solids* **2007**, *55*, 225–444.
[10] P. Fratzl, I. Burgert, H. S. Gupta, *Phys. Chem. Chem. Phys.* **2004**, *6*, 5575–5579.
[11] J. W. C. Dunlop, R. Weinkamer, P. Fratzl, *Mater. Today* **2011**, *14*, 70–78.
[12] B. L. Smith, T. E. Schaeffer, M. Viani, J. B. Thompson, N. A. Frederick, J. Kindt, A. Belcher, G. D. Stucky, D. E. Morse, P. K. Hansma, *Nature* **1999**, *399*, 761–763.
[13] Z. Y. Tang, N. A. Kotov, S. Magonov, B. Ozturk, *Nature Materials* **2003**, *2*, 413–U418.
[14] S. E. Burke, C. J. Barrett, *Biomacromolecules* **2005**, *6*, 1419–1428.
[15] S. Mann, *Angew. Chem. Int. Ed.* **2000**, *39*, 3393–3406.
[16] F. Barthelat, D. J. Zhu, *J. Mater. Res.* **2011**, *26*, 1203–1215.
[17] H. J. Gao, *Int. J. Fract.* **2006**, *138*, 101–137.
[18] L. J. Bonderer, A. R. Studart, L. J. Gauckler, *Science* **2008**, *319*, 1069–1073.
[19] S. W. Cranford, C. Ortiz, M. J. Buehler, *Soft Matter* **2010**, *6*, 4175–4188.
[20] X. H. Dai, Y. J. Zhang, Y. Guan, S. G. Yang, J. Xu, *Thin Solid Films* **2005**, *474*, 159–164.

[21] O. Mermut, J. Lefebvre, D. G. Gray, C. J. Barrett, *Macromolecules* **2003**, *36*, 8819–8824.
[22] T. Boudou, T. Crouzier, R. Auzely-Velty, K. Glinel, C. Picart, *Langmuir* **2009**, *25*, 13809–13819.
[23] a) C. Picart, B. Senger, K. Sengupta, F. Dubreuil, A. Fery, *Colloids Surf. A - Physicochemical Eng. Aspects* **2007**, *303*, 30–36; b) O. V. Lebedeva, B. S. Kim, O. I. Vinogradova, *Langmuir* **2004**, *20*, 10685–10690.
[24] O. I. Vinogradova, *J. Phys. Condens. Matter* **2004**, *16*, R1105–R1134.
[25] E. Guzman, H. Ritacco, F. Ortega, T. Svitova, C. J. Radke, R. G. Rubio, *J. Phys. Chem. B* **2009**, *113*, 7128–7137.
[26] M. Muller, *Biomacromolecules* **2001**, *2*, 262–269.
[27] R. M. Pasternack, S. R. Amy, Y. J. Chabal, *Langmuir* **2008**, *24*, 12963–12971.
[28] S. S. Shiratori, M. F. Rubner, *Macromolecules* **2000**, *33*, 4213–4219.
[29] J. B. B. Bingbing Jiang, B. Li, *Nanotechnol., Sci. Appl.* **2009**, *2*, 21–27.
[30] ASTM, *ASTM International*, **2008**.
[31] R. Rabiei, S. Bekah, F. Barthelat, *Acta Biomater.* **2010**, *6*, 4081–4089.
[32] O. Volkersen, *Luftfahrtforschung* **1938**, *15*, 41–47.
[33] M. Y. Tsai, D. W. Oplinger, J. Morton, *Int. J. Solids Structures* **1998**, *35*, 1163–1185.
[34] ASTM, *ASTM International*, **1999**.
[35] A. Khayer Dastjerdi, R. Rabiei, F. Barthelat, *J. Mech. Behav. Biomed. Mater.* **2012**; DOI: 10.1016/j.jmbbm.2012.09.004.
[36] F. Barthelat, *Philos. Trans. R. Soc. London Ser. A* **2007**, *365*, 2907–2919.
[37] S. Deville, R. K. Nalla, *Science* **2006**, *312*, 1312–1312.

Received: June 8, 2012
Published Online: September 27, 2012

